Applied Energy 101 (2013) 730–739

Contents lists available at SciVerse ScienceDirect

Applied Energy

journal homepage: www.elsevier.com/locate/apenergy

Dual-mode power regulator for photovoltaic module emulation

Younghyun Kim [a], Woojoo Lee [b], Massoud Pedram [b], Naehyuck Chang [a,*]

[a] Department of EECS/CSE, Seoul National University, Seoul, Republic of Korea
[b] Department of EE-Systems, University of Southern California, Los Angeles, CA, USA

HIGHLIGHTS

- A photovoltaic (PV) module has a dual characteristic as a voltage or a current source.
- We design a dual-mode regulator for PV module emulators.
- We develop a robust control method to perform emulation based on PV module model.
- The proposed PV emulator copes with rapid voltage or current variations.
- We show improved output quality over the entire operating range by real implementation.

ARTICLE INFO

Article history:
Received 26 October 2011
Received in revised form 13 July 2012
Accepted 24 July 2012
Available online 7 September 2012

Keywords:
Solar power
Photovoltaic module emulation
Dual-mode regulator

ABSTRACT

Photovoltaic (PV) module emulators, which can provide reproducible and controllable input power profile for a load device corresponding to different ambient conditions for a PV module, can significantly reduce the level of effort and cost for the development and optimization of the PV module, load devices, as well as interfacing power converters. In this paper, we introduce a dual-mode power regulator for the PV emulation. The dual-mode regulator consists of a voltage regulator and a current regulator, connected by two diodes for power hybridization. The circuit switches between the two regulators in order to accurately emulate the electrical output behavior of a PV module under different ambient conditions (e.g., solar irradiance, temperature) and load demands. The proposed regulator circuit provides accurate emulation results over the full operating range of the PV module by complementary use of the two regulators. We develop a robust control method for producing an accurate *I–V* curve with compensation of the loss in the circuit components. We validate the behavior of the proposed circuit and control method by Matlab/Simulink simulations and experiments. The experimental results shows that the PV emulation output is greatly improved with the proposed dual-mode regulator.

1. Introduction

Solar photovoltaic (PV) power is one of the most promising sustainable power sources with distinct advantages [1]: (i) it has no moving parts which would be subject to wear and tear, (ii) it is relatively location independent and environmentally friendly, and (iii) its core technology is experiencing rapid advancement thanks to introduction of semiconductor technologies in the PV cell manufacturing process. However, their power output varies significantly by the ambient conditions such as the solar irradiance level and temperature, and so an elaborate design of power system is needed to efficiently utilize the PV power.

Actual development and deployment of PV modules and solar-powered systems require elaborate experimental setup and experiments of a wide range, and energy efficiency is one of the most important metrics. More precisely, solar-powered systems require holistic optimization on both the PV module side and the load device side, which mandates extensive tunings based on experimental results and measurements.

The electrical output behavior of the PV module is strongly dependent on the ambient conditions, especially to the solar irradiance as shown in Fig. 1. Since the level of PV power generation is strongly dependent on the solar irradiance, it is critical for optimal development and deployment of solar-powered systems. Developing a solar-powered system involves not only development of a PV module, but also deployment of the PV module [2,3], design of associated power sources and storages [4,5], and development of its control system and operation algorithm considering the characteristics of the load device [6,7]. PV module development includes improving energy efficiency of unit PV cells, as well as determining a right design with given unit PV cells. We should carefully determine the unit PV cell type, size, series and parallel connections, and so on. However, it is difficult to achieve

* Corresponding author. Address: 1 Gwanak-gu Gwanak Road, Seoul 151-744, Republic of Korea. Tel.: +82 2 880 1836; fax: +82 2 884 1834.
E-mail addresses: yhkim@elpl.snu.ac.kr (Y. Kim), woojoole@usc.edu (W. Lee), pedram@usc.edu (M. Pedram), naehyuck@elpl.snu.ac.kr (N. Chang).

0306-2619/$ - see front matter © 2012 Elsevier Ltd. All rights reserved.
http://dx.doi.org/10.1016/j.apenergy.2012.07.025

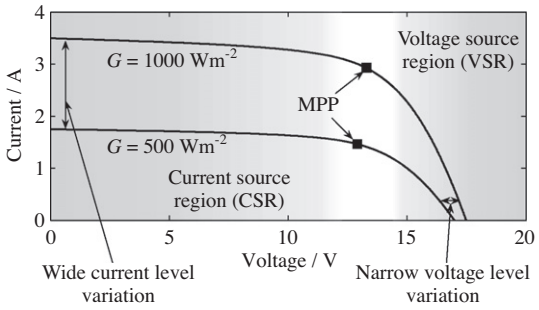

Fig. 1. *I–V* curves at two different irradiance levels. Boundary between the voltage source and current source is not definitive.

the desired design relying solely on standard parameters of PV modules [8]. Furthermore, there are too many combinations of such design parameters, and it is very difficult and highly cost-ineffective to perform experiments with the PV module under the wide range of ambient conditions in order to obtain the corresponding *I–V* characteristics and optimize the whole system including the power delivery circuit and the load device.

Instead, it will be very useful to have a PV emulator that has embedded *I–V* characteristics of the target PV modules and is able to generate the output current and voltage based on the load demand and the ambient conditions. A well-designed power emulator or simulator makes it possible to greatly reduce the amount of time and the cost of developing an optimized system [9]. A system designer can utilize the emulator or simulator to verify the PV module design integrated with the load device. It provides a high degree of freedom for experimenting different designs of a solar-powered system with any ambient condition profiles as desired, which is not possible with real PV modules. A large body of previous research has indeed introduced PV emulators that model various kinds and sizes of PV modules subject to wide-ranging ambient conditions and load demands.

A PV emulator is equipped with an adjustable power regulator, and controls the output of the regulator to accurately reproduce the *I–V* characteristics of a real PV module, which has been subjected to various ambient conditions and demands. A DC–DC converter with a current-limiting power supply can be used to simulate the *I–V* characteristics of a PV module [10], but its accuracy is not high because of the model discrepancy with the actual PV module. A reference diode or a photodiode, and a power amplifier circuit can provide higher emulation accuracy [11–13]. However, the reference diode lacks flexibility in modeling different PV modules because the emulated *I–V* characteristics of the PV module are determined by the material properties and electrical characteristics of the chosen diode. On the other hand, computational model-based PV emulators exhibit a high degree of flexibility to reconstruct an arbitrary *I–V* curve for a PV module corresponding to a desired irradiance level and ambient temperature. The PV module model calculates (predicts) the voltage and current values of the PV module at the desired ambient conditions and load demand. These values are then input to an adjustable power regulator to produce the desired electrical output [14–18]. In this paper, we focus on flexible PV emulators and thus the model-based PV emulation.

2. Motivation

The power-generation behavior of a PV module exhibit dual characteristics, i.e., sometimes the PV module's output is best modeled as a voltage source with a low internal impedance while at other times it is better modeled as a current source with a high internal impedance [19,20]. This distinction naturally gives rise to a *current source region (CSR)* and a *voltage source region (VSR)* for the PV module. When to use which model is answered based on the operating point as depicted in Fig. 1. The PV module typically shows wider output current variation in the CSR depending on the irradiance than the output voltage variation in the VSR. Furthermore, input current control is more prone to saturation than input voltage control because the current at the maximum power point is more close to the maximum output current (short circuit current) than the voltage. Due to this phenomenon, power conditioning techniques for PV modules, including the maximum power point tracking (MPPT) techniques, use a target voltage level as the set point for closed-loop feedback control rather than a current level [19,21]. For the same reason, most conventional PV emulators use only an adjustable voltage regulator to emulate the output behavior of the PV module [11,16,22,23]. They focus on the VSR, therefore, the accuracy of these emulators may be low when the PV module is operating in the CSR. In order to capture the CSR behavior of the PV module, the PV emulator in [13,15] uses a voltage regulator based on a nested-loop control mechanism, composed of an outer voltage control loop as well as an inner current control loop. However, significant current ripples are observed especially in the CSR even though output current filters are used.

Since we do not expect that load devices will always operate in such a way that the PV module remains in the VSR, the PV emulators must be capable of reproducing the real output behavior of the PV modules in its complete current range including the CSR. Even if the PV power management schemes assume operation in the VSR, it is not always possible to avoid entering the CSR. Rapid load variations may increase the current beyond the MPP before the power management scheme reacts, and sudden shading over the PV module may decrease the output and result in shifting to the CSR. For this reason, it is necessary to perform PV power management with explicit consideration on the CSR [24,25] and evaluate its behavior [26] in the CSR. Furthermore, recent research results [27,28] have decisively shown that not only the MPP but also the whole current range should be accurately modeled in order to achieve system-wide optimization of energy efficiency in a solar-powered system.

In this paper, we introduce a new circuit and control method design technique of a model-based dual-mode power regulator for PV emulation and its novel control method. The proposed dual-mode power regulator circuit is composed of an adjustable voltage regulator and an adjustable current regulator, and provides both high flexibility and high accuracy for PV emulation. We develop a robust operation method to seamlessly control the two regulators with compensating the power loss induced in the hybridization circuit. We validate the behavior of the proposed circuit and its control method with Matlab/Simulink simulation and through experiments.

3. PV module *I–V* characteristics

Fig. 2 shows a widely-used single-diode equivalent circuit model of a PV module [20]. Its *I–V* characteristic is given by

$$i_{pv} = i_L - i_d - i_{sh}, \tag{1}$$

where

$$i_L = \frac{G}{G_{STC}} \cdot i_L(G_{STC}), \tag{2}$$

$$i_d = i_0(T) \cdot \left(\exp\left(\frac{(v_{pv} + i_{pv} \cdot R_s) \cdot q}{A \cdot N_s \cdot k \cdot T} \right) - 1 \right), \tag{3}$$

$$i_{sh} = \frac{v_{pv} + i_{pv} \cdot R_s}{R_p}. \tag{4}$$

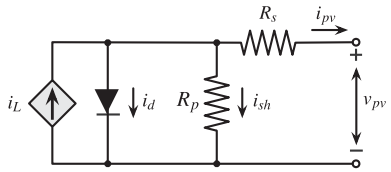

Fig. 2. Single-diode equivalent circuit model of a PV module.

The dark temperature-dependent saturation current i_0 is

$$i_0(T) = i_0(T_{STC}) \cdot \left(\frac{T}{T_{STC}}\right)^3 \cdot \exp\left(\frac{q \cdot E_g}{A \cdot N_s \cdot k} \cdot \left(\frac{1}{T_{STC}} - \frac{1}{T}\right)\right), \quad (5)$$

where v_{pv} and i_{pv} are the voltage and current of the PV module, respectively. In the above equations, G denotes the irradiance level; T is the cell temperature; N_s is the number of connected cells in series in the PV module; A is the diode ideality factor; q is the charge of an electron; E_g denotes the energy bandgap of the semiconductor and k is Boltzmann's constant. STC stands for *standard test condition* in which the irradiance level is 1000 Wm^{-2} while temperature setting is 25 °C.

Typical *I–V* characteristics of a PV module are shown in Fig. 1. A PV module basically is a current source as shown in Fig. 2, and forward biasing of the diode limits the output voltage which results in properties of a voltage source. An ideal PV module has a zero R_s and an infinite R_p, but a practical PV module has a non-zero R_s and a finite R_p. This non-ideal series and parallel resistances determine the gradients on the *I–V* curve. As mentioned above, the PV module exhibits dual behaviors which can be either a voltage source or a current source depending on the operating range. More specifically, the PV module essentially behaves as a voltage source (i.e., it supplies a constant voltage regardless of the output current) when current is low and voltage is high, and behaves as a current source (i.e., it supplies a constant current regardless of the output voltage) when voltage is low and current is high. The boundary between the VSR and CSR is not very definitive, but Refs. [19,21] define it to be the MPP of the PV module.

Consequently, the PV module shows different output behavior even with the same amount of load power variation by its operation regions. Fig. 3 illustrates how the load power variation affects the output of the PV emulator in the two different regions. The load power variation (①) results in a small voltage variation (②) and a large current variation (③) in the VRM region. In contrast, the same amount of load power variation results in a small current variation (⑤) and a large voltage variation (④) in the CSR. This implies that the PV emulators sorely based on a voltage regulator should be able to react to a small current change with a high feedback control gain in the CSR, which may result in instability in the CSR.

In this paper, we use the single-diode equivalent circuit model and assume that the MPP of the PV module sets the boundary between its VSR and CSR. However, the proposed dual-mode power regulator circuit and control method are not restricted to a particular PV module model, nor depends on the accuracy of the boundary between VSR and CSR. This is because the proposed circuit and control method are based on a computational model; the PV emulator can accommodate any PV module models, including measured *I–V* data from a real PV module. Similarly, we can apply an arbitrary boundary position between VSR and CSR.

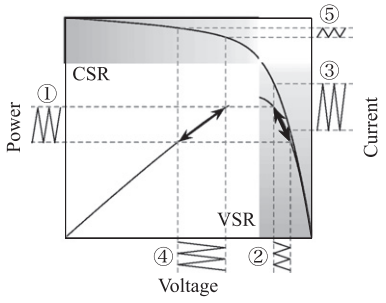

Fig. 3. Voltage and current variations in the VSR and CSR.

4. Dual-mode power regulator circuit

4.1. Modes of operation

In spite of the dual characteristics of the PV module's output, previous PV emulators have relied on only a voltage regulator to reproduce the complete output *I–V* curve of the PV module. However, in the CSR, change in the output voltage of the PV module induced by the load impedance variation can be quite large. Under these conditions, current-based control provides a better control quality, and in turn, higher PV emulation accuracy in the CSR, in the same way that voltage-based control is preferred in the VSR. Nevertheless, we do not want to use a current regulator to reproduce the entire output *I–V* curve of the PV module because it may result in low accuracy in the CSR. Even if a nested feedback controller is used (e.g., an outer voltage control loop and an inner current control loop, or vice versa) [13,15], the PV emulator will exhibit poor output controllability (and hence poor emulation accuracy) in one or the other of the two regions of operation.

Therefore, in order to reproduce the original characteristics in both the VSR and CSR, we use two separate power sources. In particular, we use a voltage regulator to generate a regulated voltage when the target PV module is operating in the VSR, and use a current regulator to generate regulated current in the CSR. We call the two operating modes of the dual-mode power regulator *voltage regulation mode (VRM)* and *current regulation mode (CRM)*. It is required to develop an elaborate power hybridization circuit which supports the VRM and CRM for the implementation of the PV emulator. A sophisticated control method also has to be designed in order to seamlessly switch between the two operating modes.

It is essential for a PV emulator to supply uninterrupted power to the load device, and so at least one of the voltage and current regulators should be turned on at all times. Instantaneously turning off the voltage regulator and turning on the current regulator, or vice versa, is not desirable because it tends to result in an instantaneous large current increase which causes current spikes. Furthermore, the power-on transient response is generally much worse than that of the set point change, and it is hard to realize seamless transition between two regulators. It is not practically feasible to turn on one regulator and turn off the other exactly at the same time, therefore we perform a make-before-break switching which has a period that both the regulators are turned on. However, different from ideal voltage and current sources, we should not simply tie up the outputs of the non-ideal voltage and current regulators because it may result in that current from the current source may flow into the voltage source. Practical voltage regulators do not allow reverse current which may cause hard failure in a power supply.

4.2. Circuit design principle

We propose a dual-mode power regulator circuit for the model-based PV emulator as shown in Fig. 4. It has adjustable voltage and current regulators whose outputs are tied together in parallel through two diodes. This parallel connection of diodes (or equivalently MOSFET-based lossless diodes) provides power hybridization preventing reverse current flow. This method has been used for power hot-swapping, and more recently, for hybridization of

heterogeneous power sources [29], but has not yet been utilized for PV emulation.

The objective of the PV emulator is to make its output voltage v_{out} and output current i_{out} faithfully track v_{pv} and i_{pv}, which are derived from the PV module model. We switch the operation mode between the VRM and CRM near the boundary of the VSR and CSR. We first define a V-to-I mapping function and an I-to-V mapping function for the given I–V curve, based on (1)–(5). These functions translate v_{pv} to i_{pv} or vice versa, for given G and T.

Fig. 5 shows three I–V curves of the target PV module model, the voltage regulator, and the current regulator. Here, the target PV module has a 17.5 V open-circuit voltage (v_{oc}) and 3.5 A short-circuit current (i_{sc}). The voltage v_{mpp} and current i_{mpp} at the MPP are 13.3 V and 2.9 A, respectively. We define v_{i2c} and i_{i2c} to be the voltage and current when the operating mode changes from the VRM to CRM, respectively, and v_{c2v} and i_{c2v} to be the voltage and current when the operating mode changes from the CRM to VRM, respectively. Both the operating points (v_{i2c}, i_{i2c}) and (v_{c2v}, i_{c2v}) are on the I–V curve, for the given G and T. These values are considered as the voltage or current limits in each operating mode. That is, the PV emulator generates the maximum output current of i_{i2c} in the VRM, and generates the maximum output voltage of v_{c2v} in the CRM.

We make VRM and CRM overlap across the boundary as shown in Fig. 5, and apply transition hysteresis. The transition hysteresis prevents frequent mode transitions between the VRM and CRM near the boundary. We make seamless transitions with the two-diode connection which allows make-before-break switching by blocking the reverse current. For example, when the operating mode switches from the VRM to CRM:

1. Keep the voltage regulator turned on and regulate output voltage v_{out} to v_{pv} while $i_{pv} < i_{i2c}$ (or equivalently, while $v_{pv} > v_{i2c}$).
2. If output current i_{out} increases and exceeds i_{i2c} (or equivalently, if v_{out} falls below v_{i2c}), turn on the current regulator (the transition point is annotated by ⓐ in Fig. 5).
3. When the current from the current regulator i_{cr} reaches i_{out}, turn off the voltage regulator and regulate output current i_{out} to i_{pv}.

The opposite is done when the operating mode switches from the CRM to VRM at ⓑ in Fig. 5; the voltage regulator is turned on first and current regulator is turned off later when the output current decreases. Both the voltage and current regulators maintain good controllability and thus high-quality output near the boundary, compared with the operating points far away from the boundary. Therefore, the proposed power hybridization and its control scheme guarantees smooth mode transition and guarantees superior output quality over the entire emulation range.

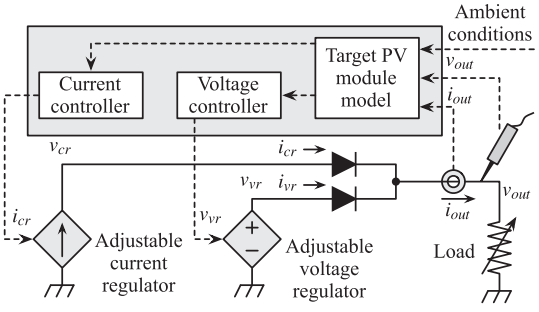

Fig. 4. Architecture of the proposed dual-mode power regulator circuit for PV emulators.

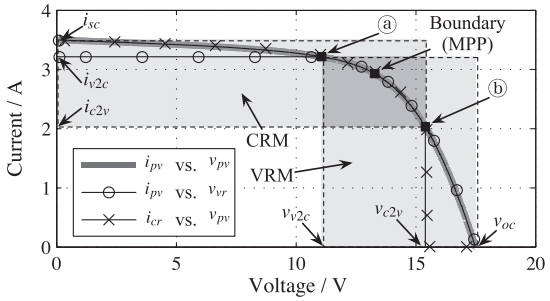

Fig. 5. I–V characteristics of the dual-mode power regulators compared with the target PV module I–V curve.

5. Dual-mode power regulator control

Fig. 6 shows a control system block diagram of the proposed dual-mode power regulator circuit. It has two separate feedback control loops for the voltage and current regulators. The voltage and current regulators are coupled with each other such that their output v_{out} and i_{out} are located on the given I–V curve of the target PV module. The V-to-I and I-to-V mapping functions in Fig. 6, which are derived from the PV module model, handle the dual-mode operation.

The output behavior of the two-diode connection is such that its output voltage is either of the higher one between the two input voltages, and only the one with the higher voltage supplies the current. If two voltages are the same, the output current is the sum of the two input currents. The voltage and current control loop regulates voltage and current at different points. The current control loop regulates i_{cr}, and the voltage regulator control loop regulates v_{out} in order to compensate the voltage drop across the diode.

The hybridization controller ('Hybrid ctrl.' in Fig. 6) is in charge of such seamless transition of the operating mode between the VRM and CRM by the load demand. The controller takes six inputs: v_{c2v}, i_{i2c}, v_{out}, i_{out}, v_{vr}, and i_{cr}, and it generates two outputs: on/off signals for the voltage and current regulators. The operating mode transition point, v_{c2v} and i_{i2c}, are derived by the transition condition block ('Transition cond.' in Fig. 6). Fig. 7 shows the functionality and behavior of the hybridization controller with a state machine. The state machine has four states: the VRM, CRM, and two intermediate states between them. The output current, i_{out}, exceeding the limit of i_{i2c} makes transition from the VRM state. This results in that the current regulator is turned on and supplies current. If its output current i_{cr} becomes equal to i_{out}, that is, the voltage regulator does not supply current anymore, the state

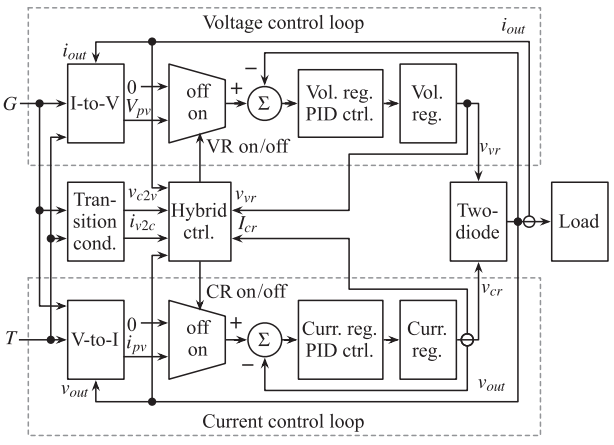

Fig. 6. Dual-mode power regulator control system block diagram.

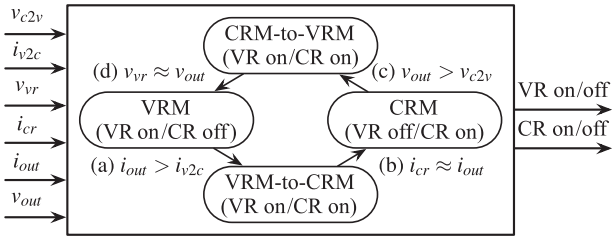

Fig. 7. State transitions and conditions of the hybridization controller (VR: voltage regulator, CR: current regulator).

machine makes a transition to the CRM state and turns off the voltage regulator. The state machine makes transition from the CRM to VRM states in the same way. We consider the distance and position of the boundary between the VRM and CRM (ⓐ and ⓑ in Fig. 5) and determine the voltage/current limit v_{c2v} and i_{v2c}. The PV emulator will switch the mode too frequently if the gap is too narrow. On the other hand, the benefit from using the dual-mode power regulator is diminished if we expand the overlapping region and the gap becomes too wide.

6. Implementation

6.1. Hardware implementation

Fig. 8 shows the implemented dual-mode regulator-based PV emulator board. Fig. 9 shows the circuit schematic diagram of the proposed PV emulator. We use a low dropout (LDO) linear regulator LT1083 from Linear Technology as the voltage regulator. Switching regulators have a higher efficiency in general, but they are inherently subject to switching noise and voltage ripples even the load is constant. Since a PV module does not create any noisy ripples on its voltage and current, we use a linear regulator for the voltage source to eliminate them.

Power dissipated in a linear regulator is proportional to the dropout (voltage difference between the input and output). The dropout may be large in a wide output-adjustable regulator, and this results in a high heat dissipation. We implement a voltage pre-regulating circuit [30] for the input of the linear regulator to mitigate the heat dissipation. It automatically adjusts the input voltage to be higher than the output voltage by the required minimum dropout to minimize the heat dissipation, and allows a large amount of current from the linear regulator. The implemented voltage regulator is capable of supplying 1.2–21.8 V of output voltage with 12-bit resolution and up to 5.0 A of output current. However, the proposed dual-mode regulator architecture is not restricted to which type of regulator is used. We may use a high-efficiency switching regulator instead of the linear regulator as the voltage/current source to reduce its power dissipation for high-power PV emulation.

We implement a precision 10-bit resolution current regulator introduced in [31] for the current regulator also with the LT1083. The maximum available output current is 5.0 A up to 16.5 V, and it decreases as the output voltage increases up to 19.5 V. This does not limit the power capacity of the emulator since the current regulator generates a high current in the CRM where the voltage is low.

Due to the physical constraints of the components, the PV emulator's output voltage and current cannot span unlimitedly. Table 1 shows the voltage and current output ranges of the regulators. The range of operation of the regulators while performing the emulation is dependent not only on their physical capability, but also the I–V characteristic of emulating PV module. That is, the minimum output voltage that the voltage regulator generates is v_{v2c}, and the minimum output current that the current regulator generates is i_{c2v}, which vary depending on the target of emulation, as illustrated in Fig. 5.

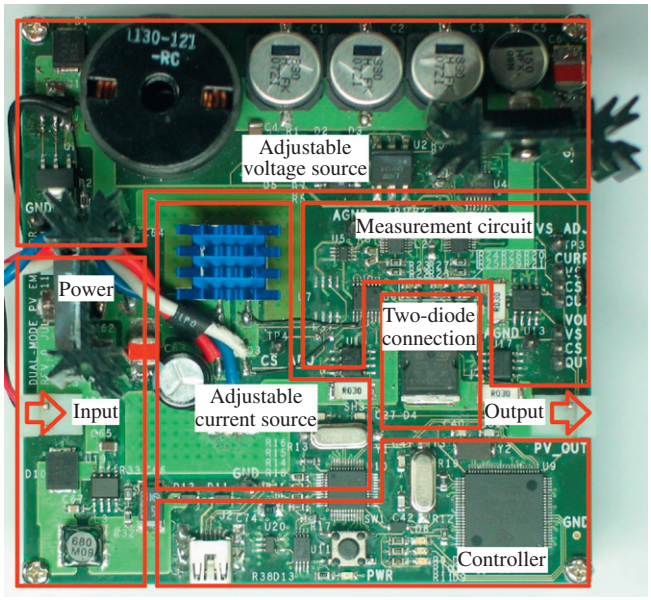

Fig. 8. Implemented dual-mode regulator-based PV emulator board.

The two regulators are connected through a Schottky diode array STPS20L45C from STMicroelectronics. It has a forward voltage drop in a range of 0.4–0.6 V varying depending on the temperature and forward current. It is described in the datasheet that the diode will have around 0.3 W of conduction loss at 1 A forward current due to the on-resistance. Therefore, we compensate the voltage drop and resulting power loss through a feedback control as discussed in Section 5.

The controller is Stellaris LM3S3748 microprocessor with ARM Corex-M3 core running at 50 MHz. We use a real-time operating system μC-OS II to implement the controller described in Section 5. The control task performs PID control at 1 kHz frequency. PID parameters are critical for fast response and stable operation of the PID controller to disturbances. We carefully set the PID parameters so that the voltage and current regulators have a fast response to the load variation and generate stable voltage and current output. We perform PID parameter tuning through extensive experiments and apply gain scheduling to achieve the best performance for the voltage and current regulators. The gain scheduling adjusts the PID parameters depending on the operation range in order to cope with the non-linear behavior. We divide the operation range into several subranges and tune the PID parameters for each subrange.

6.2. PV module modeling

We use a PV module which generates up to 39 W at a 1000 Wm^{-2} irradiance and a 27 °C ambient temperature as a reference. Representative characteristics of the module are shown in Table 2, and the entire reference I–V curve of the target PV module is as shown in Fig. 5.

Converting v_{pv} to i_{pv} or i_{pv} to v_{pv} requires iterative computations such as Newton–Raphson method to converge. An embedded processor is not suitable for such a computation-extensive workload, and so it is not practical to implement online conversion for the V-to-I and I-to-V mapping function. Rather, we build mapping tables of I–V curves of some G values offline, and perform a spline interpolation online. The mapping tables have a granularity so that

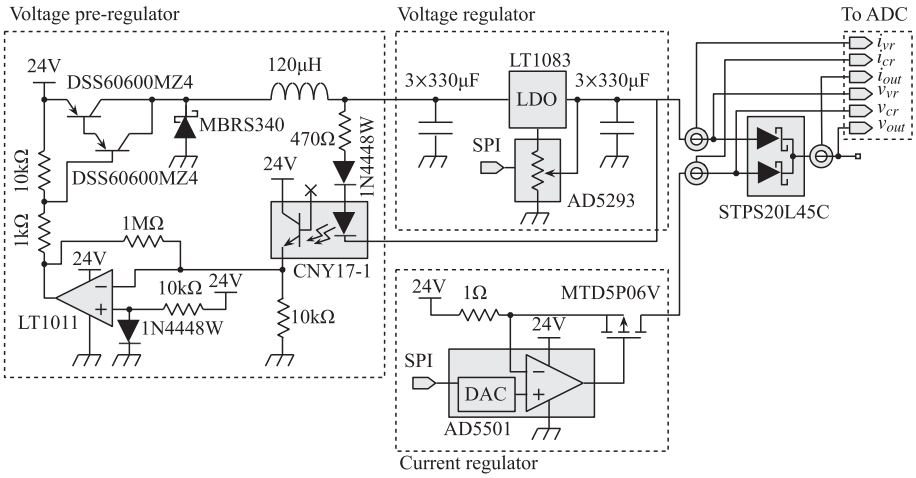

Fig. 9. Circuit schematic diagram of the PV emulator design.

Table 1
Output specification of the implemented PV emulator. All values are measured at the output terminal.

Regulator	Output	Conditions	Min.	Max.	Unit
Voltage regulator	Voltage	i_{out} = 2.0 A	1.2	21.8	V
	Current	v_{out} = 10.0 V	–	5.0	A
	Power	v_{out} = 21.8 V	–	109.0	W
		i_{out} = 5.0 A			
Current regulator	Voltage	i_{out} = 2.0 A	–	19.5	V
	Current	v_{out} = 10.0 V	0.0	5.0	A
	Power	v_{out} = 16.5 V	–	82.5	W
		i_{out} = 5.0 A			

Table 2
Reference characteristics of the target solar module.

Parameter	Value	Unit
Reference solar irradiance (G_0)	1000	Wm^{-2}
Reference temperature (T_0)	27	°C
Open circuit voltage (v_{oc})	17.5	V
Short circuit current (i_{sc})	3.5	A
Maximum power (p_{mpp})	38.9	W
Voltage at maximum power (v_{mpp})	13.3	V
Current at maximum power (i_{mpp})	2.9	A

the PV emulator can fully utilize the high-accuracy voltage and current regulators. That is, since the output of the voltage regulator and current regulator has 12-bit and 10-bit resolution, respectively, the *I*-to-*V* mapping table and *V*-to-*I* mapping table has more than 4096 and 1024 entries, respectively.

7. Experiments

7.1. Experimental setup

We setup experimental environment as shown in Fig. 10. The implemented PV emulator is connected to the adjustable electronic load Kikusui PLZ334WL which can consume up to 300 W of power. The currents and voltages of the regulators and output are measured with a DAQ from the National Instruments. All the system including the PV emulator, electronic load, and DAQ is controlled by a customized automated tool.

7.2. Experimental results

7.2.1. PV module I–V characteristics

We first measure the output of the target PV module to compare the voltage and current variations in the VRM and CRM regions. Table 3 is the voltage and current variations of the target PV module caused by load power variations in the VRM and CRM regions. Refer to Fig. 3 which graphically illustrates the voltage and current variations caused by the power variation. We measure the voltage variation (② and ④) and current variation (③ and ⑤) while changing the load power (①) in a range of 40–60% of the maximum power for the given irradiance. Table 3 presents the range of voltage and current variations in each region and the normalized value Δ_{norm} to the maximum voltage and maximum current, which are v_{oc} and i_{sc}, respectively. This definitely shows that using an appropriate power regulator results in only 1–3% output variations, otherwise it suffers from 13–15% output variations. This phenomenon becomes more clear when the operating point is near the maximum voltage (open-circuit) or maximum current (short-circuit). This confirms the dual characteristic of the PV module and shows the potential benefits of using two different regulators for PV emulation.

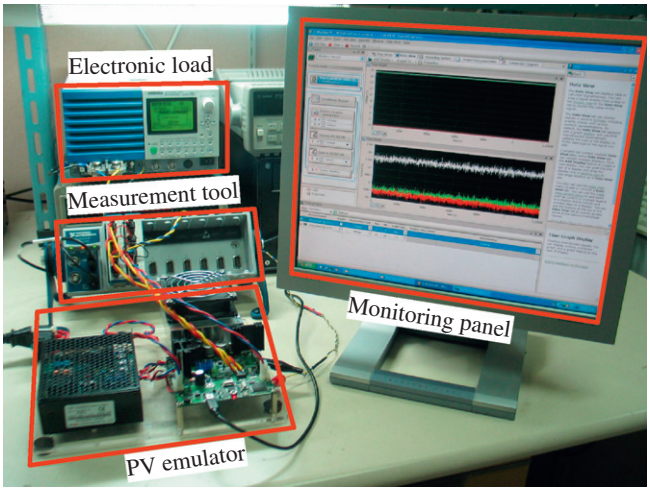

Fig. 10. Experimental setup.

Table 3
Voltage and current variations by the load power variation of 40–60% of the maximum power at 1000 and 500 Wm^{-2}.

G (Wm^{-2})	Region	Output	Marker in Fig. 3	Range	Δ_{norm}(%)
1000	VSR	Voltage	②	16.2–16.7 V	2.9
		Current	③	0.93–1.44 A	14.6
	CSR	Voltage	④	4.5–6.9 V	13.7
		Current	⑤	3.38–3.43 A	1.4
500	VSR	Voltage	②	15.7–16.2 V	2.9
		Current	③	0.47–0.72 A	14.3
	CSR	Voltage	④	4.4–6.7 V	13.5
		Current	⑤	1.69–1.71 A	1.1

7.2.2. Matlab/Simulink simulation

We first validate the functionality of the proposed circuit and the control method with Matalb/Simulink simulation. Through the simulation, we show that the proposed circuit well performs the PV emulation, and present the resulting voltage, current, and power behavior. We use adjustable voltage and current regulator models, diode models, and resistive load models from the Matlab/Simulink Simscape library. Without loss of generality, we use a pre-measured PV module *I–V* curve at a given irradiance level and temperature for demonstration purpose.

First, we define the transition conditions in Fig. 7. We define i_{v2c} in (a) and v_{c2v} in (c) as follows:

$$i_{v2c} = (v_{mpp} + v_{oc})/2, \tag{6}$$
$$v_{c2v} = (i_{mpp} + i_{sc})/2. \tag{7}$$

We consider that $v_{vr} \approx v_{out}$ in (b) and $i_{cr} \approx i_{out}$ in (d) when the error is less than 0.1%. These conditions are empirically determined based on the observation on the *I–V* curve of the target PV module.

Fig. 11 shows the *I–V* curves, *P–V* curves, and *P–I* curves of the PV module model, voltage regulator, current regulator, and emulator output. Fig. 11a and b shows the two cases such that the operating point changes in two different directions, respectively, which are denoted by a gray arrow. It demonstrates the hybridization controller described in Section 5 is functioning as expected. The operating mode transition occurs when the output voltage reaches to v_{v2c} in the VRM in Fig. 11a or when the output current reaches to i_{c2v} in the CRM in Fig. 11b. We see from the *I–V* curves that the voltage output of the voltage and current regulators is higher than v_{pv} (shifted to higher than v_{pv}) as a result of the feedback control to compensate the diode forward bias voltage drop of 0.6 V and the diode on-resistance of 0.3 Ω. In spite of the steep *I–V* curve at the transition, the resultant PV emulator output *I–V* characteristic well matches with that of the PV module model thanks to the use of two-diode hybridization circuit and control.

7.2.3. I–V characteristics

Now that we have validated the functionality through simulation, we present the measurement results obtained from the physical experimental setup introduced in Section 7.1. We show the output quality of the proposed PV emulator compared with two conventional voltage or current regulator-based PV emulators. We turn off the current or voltage regulator to generate the output of voltage regulator-based PV emulator or current regulator-based emulator, respectively.

Fig. 12a–c shows the *I–V* curves measured from the three PV emulators based on the voltage regulator, current regulator, and dual-mode regulator, respectively. We measure the voltage and current while changing the load from the with period of 30 s. The load changes between zero (open circuit) to the value that makes the output 2 V, which is close to the minimum output

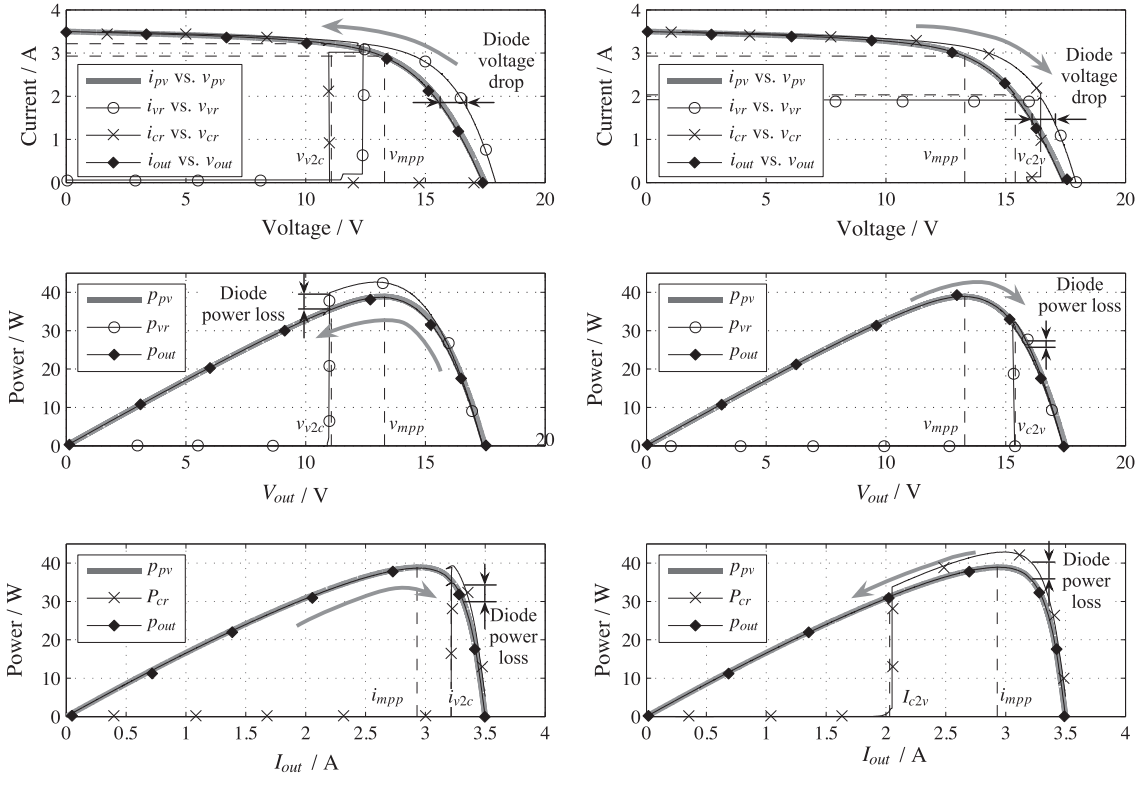

(a) Transition from the VRM to CRM

(b) Transition from the CRM to VRM

Fig. 11. *I–V*, *P–V*, and *P–I* curves of the voltage regulator, current regulator, and emulator output, compare with the PV module model while transiting (a) from the VRM to CRM and (b) from the CRM to VRM.

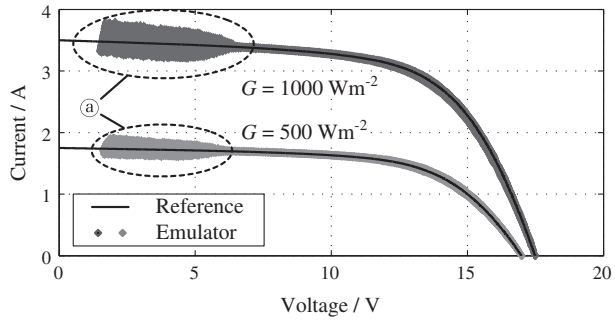

(a) Voltage regulator-based emulation

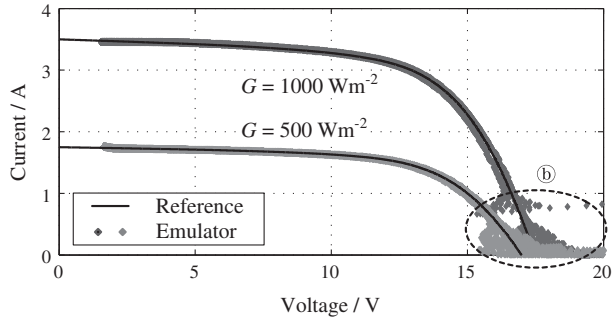

(b) Current regulator-based emulation

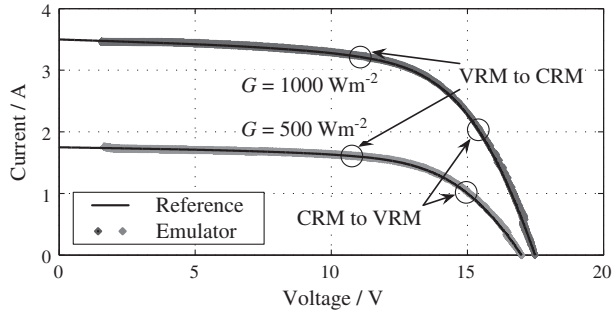

(c) Dual-mode regulator-based emulation

Fig. 12. *I–V* curves of PV emulation based on three regulators: (a) voltage regulator, (b) current regulator, and (c) dual-mode regulator.

voltage described in Table 1. In each figure, the solid line denotes the desired output *I–V* characteristic according to the PV module model, and the markers denote the measured points.

In Fig. 12a and b, it is definite that the output of the regulators are not as expected in some operating range. More specifically, the voltage regulator fails to generate the desired voltage in the CSR as annotated by ⓐ. Similarly, the current regulator fails to generate the desired current in the VSR as annotated by ⓑ. This is not because the regulators are not capable of generating high power in those regions, but because the output voltage or current variation is too rapid for the regulator to follow the output change. The power output capability of the regulators is enough to generate the voltage and current on the target *I–V* curves as presented in Table 1. For example, the voltage regulator can stably supply up to 5 A at 10 V, but the *I–V* curve of 500 Wm^{-2} in Fig. 12a shows unstable output at low current and low voltage range below 1.8 A and 7 V. In contrast, the output of the dual-mode regulator is in a good quality as shown in Fig. 12c. The output in the VSR is as good as that of the voltage regulator-based emulator, and the output in the CSR is as good as that of the current regulator-based emulator.

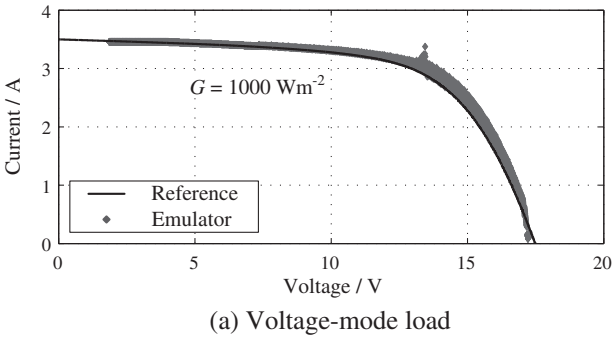

(a) Voltage-mode load

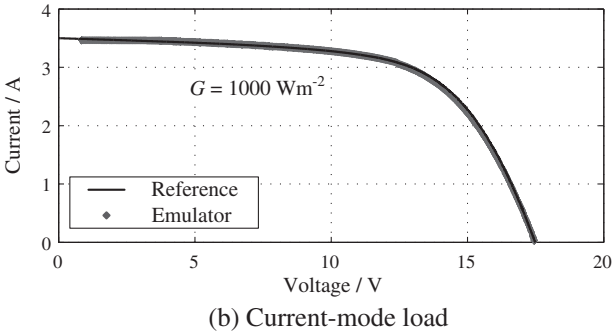

(b) Current-mode load

Fig. 13. *I–V* curves of PV emulation for (a) a voltage-mode load and (b) a current-mode load.

In practice, a load device connected to a PV module is not only a resistance-mode load, but may be a voltage-mode, current-mode, or combination of them. Therefore, we show that the proposed dual-mode PV emulator shows a good stability over all operating range not only for the resistance-mode load as shown in Fig. 12c, but also for voltage- and current-mode loads. Fig. 13a and b shows *I–V* curves when a voltage- and current-mode load is applied, respectively. We can see that both *I–V* curves for the voltage- and current-mode loads exhibit good consistency with the reference *I–V* curve.

7.2.4. Mode transitions

Fig. 14 shows the voltage and current output variations of the voltage regulator, current regulator, and emulator output when the load changes. This is a representation of the data in Fig. 12c

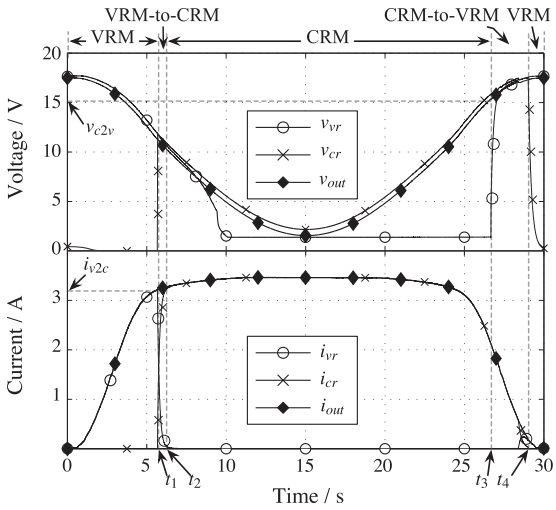

Fig. 14. Output of the voltage and current regulators for varying load.

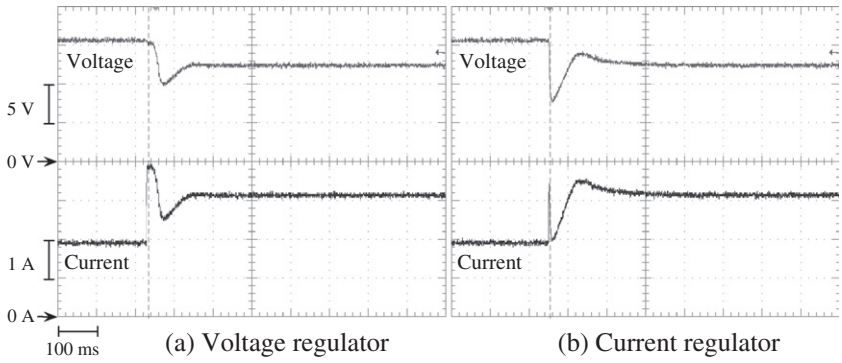

Fig. 15. Voltage and current variance for step change of load resistance from 8.3 Ω to 4.0 Ω.

in a time axis. We apply a variable load starting from a zero load (open-circuit) to a very low resistance load (near short-circuit), and back to a zero load.

It starts in the VRM state because the load is zero. Current draw increases, and at t_1, the output current i_{out} reaches i_{v2c} which is the current limit of the voltage regulator. The operating mode changes from the VRM to VRM-to-CRM state, in which i_{cr} gradually increases, and i_{vr} gradually decreases. Finally, i_{cr} reaches to i_{out} at t_2, and the voltage regulator is turned off, by entering the CRM state. We see that the operating mode transition is seamlessly performed, and the output voltage v_{out} and current i_{out} are stably maintained during the transition. The hybrid controller performs the opposite when the operation mode changes from the CRM to VRM. The output voltage v_{out} increases and current i_{out} decreases until it reaches v_{c2v} at t_3. The controller enters the CRM-to-VRM state and the voltage regulator is turned on. When the output voltage of the voltage regulator reaches v_{out} at t_4, the current regulator is turned off by entering the VRM state.

Next, we show the PV emulator's transient response to a step load change. A PV emulator should be able to change its operating point rapidly when the load changes. Due to the control hysteresis, the same operating point can be regulated by either voltage or current regulator, especially near the MPP. Therefore, we apply a step change of the load resistance and observe the voltage and current variations [21]. The step response of the voltage regulator and current regulator is shown in Fig. 15a and b, respectively. The MPP is at 2.9 A and 13.3 A, which corresponds to 4.5 Ω. The load resistance is first 8.3 Ω and the PV emulator output is 1.9 A at 15.6 V. We decrease the resistance to 4.0 Ω and the operating point changes to 3.1 A at 12.4 V. Both the voltage and current converters to the desired operating point within about 100 ms.

8. Conclusions

High accuracy emulation of PV modules significantly reduces cost and effort for solar-powered system development. The quality of emulation is largely dependent on the PV module model as well as the power regulator that generates the output. The PV modules have two different output behavior as a voltage source and a current source, by the ambient conditions and load behavior. Conventional control methods, such as voltage regulator only or voltage regulator with an inner current feedback loop, do not provide high-accuracy output for the entire range of the *I–V* characteristics.

The proposed power regulation method is hybrid of a voltage and a current source, connected with a two-diode hybridization circuit. The primary advantage of the proposed circuit is symmetrical characteristics in terms of controllability and accuracy both in the voltage and current source regions. We provide a novel control method taking into account a fact that maximum power point tracking (MPPT) is mostly done at near the boundary point. We perform a Matlab/Simulink simulation and validated of the proposed power regulation circuit. We also measured the output of implemented PV emulator and compared with conventional methods to confirm its efficacy.

Acknowledgements

This work is supported by the Mid-Career Researcher Program through NRF Grant funded by the Ministry of Education, Science and Technology (MEST) (No. 2010-0017680), the Smart IT Convergence System Research Center funded by the MEST as Global Frontier Project (SIRC-2011-0031851), the Brain Korea 21 Project and a grant from the U.S. National Science Foundation. The ICT at Seoul National University provides research facilities for this study.

References

[1] Carrasco J, Franquelo L, Bialasiewicz J, Galvan E, Guisado R, Prats M, et al. Power-electronic systems for the grid integration of renewable energy sources: a survey. IEEE Trans Ind Electron 2006;53(4):1002–16.
[2] Kostić LT, Pavlović T, Pavlović Z. Optimal design of orientation of PV/T collector with reflectors. Appl Energy 2010;87(10):3023–9.
[3] Şenpinar A, Cebeci M. Evaluation of power output for fixed and two-axis tracking PVarrays. Appl Energy 2012;92(0):677–85.
[4] Dufo-López R, Bernal-Agustn JL, Yusta-Loyo JM, Domnguez-Navarro JA, Ramrez-Rosado IJ, Lujano J, et al. Multi-objective optimization minimizing cost and life cycle emissions of stand-alone PV-wind-diesel systems with batteries storage. Appl Energy 2011;88(11):4033–41.
[5] Al-Alili A, Hwang Y, Radermacher R, Kubo I. high efficiency solar air conditioner using concentrating photovoltaic/thermal collectors. Appl Energy 88.
[6] Akkaya R, Kulaksiz A. A microcontroller-based stand-alone photovoltaic power system for residential appliances. Appl Energy 2004;78(4):419–31.
[7] Sallem S, Chaabene M, Kamoun M. Energy management algorithm for an optimum control of a photovoltaic water pumping system. Appl Energy 2009;86(12):2671–80.
[8] Sharma R, Tiwari G. Technical performance evaluation of stand-alone photovoltaic array for outdoor field conditions of new delhi. Appl Energy 2012;92(0):644–52.
[9] Chen M, Rincón-Mora G. Accurate electrical battery model capable of predicting runtime and *I–V* performance. IEEE Trans Energy Convers 2006;21(2):504–11.
[10] Lopes L, Lienhardt A-M. A simplified nonlinear power source for simulating PV panels. In: Proceedings of power electronics specialist conference (PESC), vol. 4; 2003. p. 1729–34.
[11] Nagayoshi H. *I–V* curve simulation by multi-module simulator using *I–V* magnifier circuit. Solar Energy Mater Solar Cells 2004;82(1–2):159–67.
[12] Armstrong S, Lee C, Hurley W. Investigation of the harmonic response of a photovoltaic system with a solar emulator. In: Proceedings of European conference on power electronics and applications; 2005. p. 1–8.
[13] Koran A, Sano K, Kim R-Y, Lai J-S. Design of a photovoltaic simulator with a novel reference signal generator and two-stage LC output filter. IEEE Trans Power Electron 2010;25(5):1331–8.
[14] Zeng Q, Song P, Chang L. A photovoltaic simulator based on DC chopper. In: Proceedings of Canadian conference on electrical and computer engineering (CCECE), vol. 1; 2002. p. 257–61.

[15] Sanchis P, Echeverria I, Ursua A, Alonso O, Gubia E, Marroyo L. Electronic converter for the analysis of photovoltaic arrays and inverters. In: Proceedings of power electronics specialist conference (PESC), vol. 4; 2003. p. 1748–53.
[16] Cirrincione M, Di Piazza M, Marsala G, Pucci M, Vitale G. Real time simulation of renewable sources by model-based control of DC/DC converters. In: Proceedings of international symposium on industrial electronics (ISIE); 2008. p. 1548–55.
[17] Piazza MCD, Vitale G. Photovoltaic field emulation including dynamic and partial shadow conditions. Appl Energy 2010;87(3):814–23.
[18] Lee W, Kim Y, Wang Y, Chang N, Pedram M, Han S. Versatile high-fidelity photovoltaic module emulation system. In: Proceedings of international symposium on low power electronics and design (ISLPED); 2011. p. 91–6.
[19] Xiao W, Dunford W, Palmer P, Capel A. Regulation of photovoltaic voltage. IEEE Trans Ind Electron 2007;54(3):1365–74.
[20] Villalva M, Gazoli J, Filho E. Comprehensive approach to modeling and simulation of photovoltaic arrays. IEEE Trans Power Electron 2009; 24(5):1198–208.
[21] Durán E, Andújar J, Segura F, Barragán A. A high-flexibility DC load for fuel cell and solar arrays power sources based on DC–DC converters. Appl Energy 2011; 88(5):1690–702.
[22] Di Piazza M, Pucci M, Ragusa A, Vitale G. Analytical versus neural real-time simulation of a photovoltaic generator based on a DC–DC converter. IEEE Trans Ind Appl 2010;46(6):2501–10.
[23] Ziming Z, Jianwen Z, Haimeng S, Gang W, Xiwen H, Shi Z. Research on photovolta array emulator system based on a novel zero-voltage zero-current switching converterer. In: Proceedings of Asia–Pacific power and energy engineering conference (APPEEC); 2010. p. 1–4.
[24] Shao H, Tsui C-Y, Ki W-H. An inductor-less microsolar power management system design for energy harvesting applications. In: Proceedings of international symposium on circuits and systems; 2007. p. 1353–6.
[25] Libo W, Zhengming Z, Jianzheng L. A single-stage three-phase grid-connected photovoltaic system with modified mppt method and reactive power compensation. IEEE Trans Energy Convers 2007;22(4):881–6.
[26] Lee JH, Bae H, Cho BH. Advanced incremental conductance MPPT algorithm with a variable step size. In: Proceedings of international power electronics and motion control conference (EPE-PEMC); 2006. p. 603–7.
[27] Kim Y, Chang N, Wang Y, Pedram M. Maximum power transfer tracking for a photovoltaic-supercapacitor energy system. In: Proceedings of international symposium on low power electronics and design (ISLPED); 2010. p. 307–12.
[28] Lu C, Raghunathan V, Roy K. Maximum power point considerations in micro-scale solar energy harvesting systems. In: Proceedings of international symposium on circuits and systems (ISCAS); 2010. p. 273–6.
[29] Kim Y, Shin D, Seo J, Chang N, Cho H, Kim Y, et al. System integration of a portable direct methanol fuel cell and a battery hybrid. Int J Hydrogen Energy 2010;35(11):5621–37.
[30] Linear Technology. LT1083: 7.5A, 5A, 3A low dropout positive adjustable regulators.
[31] Neubauer J. Precision current source is software-programmable. EDN 2004:72.